

# Inherent flexibility determines the transition mechanisms of the EF-hands of Calmodulin

Swarnendu Tripathi and John J. Portman

*Department of Physics, Kent State University, Kent, OH 44242*

(Dated: October 14, 2021)

## Abstract

We explore how inherent flexibility of a protein molecule influences the mechanism controlling the kinetics of allosteric transitions using a variational model inspired from work in protein folding. The striking differences in the predicted transition mechanism for the opening of the two domains of calmodulin (CaM) emphasizes that inherent flexibility is key to understanding the complex conformational changes that occur in proteins. In particular, the C-terminal domain of CaM (cCaM) which is inherently less flexible than its N-terminal domain (nCaM) reveals “cracking” or local partial unfolding during the open/closed transition. This result is in harmony with the picture that cracking relieves local stresses due to conformational deformations of a sufficiently rigid protein. We also compare the conformational transition in a recently studied “even-odd” paired fragment of CaM. Our results rationalize the different relative binding affinities of the EF-hands in the engineered fragment compared to the intact “odd-even” paired EF-hands (nCaM and cCaM) in terms of changes in flexibility along the transition route. Aside from elucidating general theoretical ideas about the cracking mechanism, these studies also emphasize how the remarkable intrinsic plasticity of CaM underlies conformational dynamics essential for its diverse functions.

## INTRODUCTION

To understand protein function, it is often essential to characterize large conformational changes that occur upon ligand binding. Within the population-shift mechanism of allosteric conformational change,<sup>1</sup> the bound complex is formed when a ligand selects and stabilizes a weakly populated conformational ensemble from the kinetically accessible states of the unbound folded protein. Consequently, the kinetics of large scale conformational transitions between two meta-stable states are determined largely by the inherent conformational dynamics within the folded state free energy basin. Such conformational dynamics imply an inherent flexibility or “intrinsic plasticity” of the folded state. In this paper, we focus on how this inherent flexibility of a protein molecule influences the mechanism controlling the kinetics of allosteric transitions. There are a couple of possible scenarios for the transition mechanism in terms of changes in conformational flexibility. One possibility is that the flexibility adjusts smoothly to the conformation deformation between two specific meta-stable states in the free energy surface. In this case, the inherent flexibility of the protein remains relatively constant if the meta-stable states have similar flexibilities or else changes smoothly between the flexibilities of the meta-stable states if the flexibilities are different. Another possible mechanism, called “cracking”,<sup>2</sup> has recently been proposed as an alternative mechanism that may be important in some conformational transitions. In terms of conformational flexibility, cracking involves non-monotonic changes in flexibility along the transitions route. In particular, the flexibility of specific regions of the protein may transiently increase through local unfolding. As explained in Ref.2, local unfolding can relieve specific areas of high stress during conformational deformations that would result in high free energy barriers if the protein remained uniformly folded throughout the transition.

In the model developed to explore this idea, cracking is introduced directly into the formalism as means to incorporate nonlinear elasticity in an otherwise harmonic description of conformational fluctuations (i.e., normal modes).<sup>2,3</sup> This work clearly shows that local unfolding can dramatically lower predicted free energy barriers between local free energy minima and hence facilitates faster kinetics. In contrast, the variational model developed in the present work does not assume cracking from the outset. The evidence of cracking here arises entirely from the analysis of the local changes in flexibility along transition routes predicted by an inherently non-linear model of conformational transitions. Our results are

thus an independent verification of the ideas and formalism developed in the model presented in Ref.2,3.

Cracking does not occur in all conformational transitions, but even when it does, the average conformations of the local minima in the free energy may show little signs that local unfolding is involved.<sup>2</sup> Instead, cracking is a subtle consequence of the nature of the conformational deformation required to connect the two states. Since cracking is akin to folding of the whole protein albeit on a constrained and local scale, it is reasonable to ask if some insight appropriated from the success of the energy landscape theory of protein folding<sup>4</sup> can help to anticipate when cracking is likely to be important in conformational transitions between two distinct folded conformations. One motivation for the work in this paper is to investigate if the cracking mechanism of conformational transitions, like the mechanism for folding of two state proteins,<sup>5</sup> is determined by structural topology of the two meta-stable states. To address this question we study the conformational transitions of the open and closed conformations of the two homologous domains of calmodulin (CaM) as well as a fragment of CaM involving parts of both domains. Aside from general theoretical implications, the results presented in this paper are interesting from the point of view of understanding the well-known and intensely studied thermodynamic differences between the two domains of CaM.<sup>6,7</sup>

Our approach is based on a coarse-grained variational model previously developed to characterize protein folding.<sup>8</sup> This model is in harmony with several recent coarse-grained simulations based on a folded-state biased interaction potential that interpolates between the contact maps of the meta-stable states.<sup>9,10,11,12,13,14</sup> Interestingly some of these recently proposed coarse-grained model for protein conformational transition can also capture the cracking or local partial unfolding during transition<sup>10,12,13</sup>. In this paper we compare the detailed predicted transition routes for the open/closed conformational change of the C-terminal domain of Calmodulin (cCaM) with that of the N-terminal domain of CaM (nCaM). The open and closed state of each domain is shown in Fig. 1(a-b). We find that although the nCaM and cCaM have similar structures, the calculated transition routes predict that the cracking is essential only in cCaM. It is well established that the two domains differ in flexibility as well as binding affinity for  $\text{Ca}^{2+}$ .<sup>6,7</sup> These properties are not determined by topology (since they are the same) but ultimately by more subtle structural differences encoded in the sequence of the two domains. Our results suggest that nCaM is flexible enough that

cracking is not necessary to relieve stress during the conformational change, while the cCaM is relatively rigid so that cracking is involved in essentially the same conformational change. In addition, we investigate the conflicting  $\text{Ca}^{2+}$  binding mechanism in the “odd-even” and “even-odd” paired EF-hands between the two domains of CaM [shown in Fig. 1(c)]. Our study indicates that the highly flexible central linker region locally unfolds before folding into a stable  $\alpha$ -helix. Our predicted transition mechanism rationalizes the sequential  $\text{Ca}^{2+}$  binding in CaM2/3.<sup>15</sup> in terms of the differences in conformational flexibility of  $\text{Ca}^{2+}$ -binding loops in CaM2/3. Finally, we address how our comparative study of conformational transitions in “odd-even” and “even-odd” paired EF-hands reveals the interplay between intrinsic plasticity, target binding affinity, and function of CaM.

## RESULTS

**Conformational Flexibility of the CaM Domains.** We first compare the inherent flexibility of the two domains of CaM by calculating the mean-square fluctuations  $\mathcal{B}_i$  for each residue in the nCaM and cCaM for the open/closed conformational transitions of each domain. Fig. 2(a) shows  $\mathcal{B}_i$  along the open/closed conformational transition for each residue of nCaM from our very recent studies.<sup>16</sup> The magnitude of the fluctuations for each residue of cCaM for the open/closed transition route is shown in Fig. 3(a). Comparison of Fig. 2(a) and 3(a) show that although the binding loops and helix-linker in both domains are very flexible, the apo (closed)-nCaM is inherently more flexible than apo (closed)-cCaM. For nCaM, the flexibility of the the binding loops I and II and the B/C helix-linker between EF-hands 1 and 2 decreases upon domain opening. Similarly, the flexibility of the  $\text{Ca}^{2+}$  binding loops III and IV decreases considerably during the opening of cCaM. The fluctuations of the F/G helix-linker between EF-hands 3 and 4 has different behavior along the transition route. The flexibility of this region of the protein increases to a relatively high flexibility in the intermediate states between the open and closed conformations before reducing the flexibility of the folded open conformation. (Fig. 3(a)). We also note that the F/G helix-linker in the open structure is more flexible than in the closed structure. The calculated conformational flexibility suggests that unlike the B/C helix-linker in the apo (closed)-nCaM the F/G helix-linker in the apo (closed)-cCaM is relatively less flexible. The increase and then decrease in flexibility of the F/G helix-linker during the domain opening of cCaM indicates there is

cracking or local partial unfolding in this less flexible F/G helix-linker which facilitates the conformational change by increasing its flexibility near the transition state ensemble. [See the change in fluctuations of the F/G helix-linker during domain opening in Fig. 3(a)] The model also predicts that binding loop II in CaM has the highest flexibility in comparison with other binding loops. [Compare the flexibility of the binding loops in Fig. 2(a) and 3(a).] This result agrees with a recent molecular dynamics simulation study of CaM D129N mutant, where the binding loop II consistently exhibited higher mobility than the other three  $\text{Ca}^{2+}$  binding loops.<sup>17</sup>

**Cracking in the Conformational Transition of cCaM.** To compare the conformational flexibility of the two CaM domains in more detail we have plotted the change in fluctuations  $\mathcal{B}_i$  for some specific residues in Fig. 4. Each binding loop of CaM has 12 residues with a conserved Glutamate (Glu) residue in the 4<sup>th</sup> position of the loops. In Fig. 4 we show Glu23 and Glu59 from binding loops I and II of nCaM, respectively. Also, Glu96 and Glu132 from binding loops III and IV of cCaM, respectively. In Fig. 4, we also included the Glycine (Gly) and Aspartic (Asp) residues from the helix-linker at position 45 and 118 of the nCaM and cCaM, respectively. [Note that all these six residues show sharp peaks in Fig. 2(a) and 3(a).] Residue Asp118 of the F/G helix-linker from cCaM shows very different behavior relative to the rest of the residues in Fig. 4. Residue Asp118 shows highest  $\mathcal{B}_i$  near the transition state at  $\alpha_0 = 0.4$  whereas  $\mathcal{B}_i$  of all the other residues shown decrease monotonically during closed to open transition with the closed conformation having the largest fluctuations. This result supports that this increase in flexibility of the helix-linker region in cCaM near the transition state is due to some local transient unfolding or cracking. For further analysis of cracking in the cCaM we have also compared the contact pair potential energy  $u_{ij}$  for residues Glu45 and Asp118 from the helix-linker of nCaM and cCaM respectively along the transition route. Fig. 5 shows that for residue Asp118,  $u_{ij}$  increases in the transition state and therefore cracking occurs. On the other hand,  $u_{ij}$  for residue Glu45 from the helix-linker of nCaM decreases in the transition state. This striking difference in  $u_{ij}$  implies that the increase in contact energy of the F/G helix-linker during opening of cCaM leads to some transient cracking in this region near the transition state which further enhances the inherent flexibility of this linker during the open/closed conformational change.

**Open/Closed Transition Mechanism of the CaM Domains.** To further elucidate the predicted conformational transition mechanisms of domain opening in CaM, we consider

a structural order parameter that measures the similarity to the open (holo) or closed (apo) state conformations,  $\Delta\overline{\rho}_i$ , described in the Methods section. This order parameter is defined such that  $\Delta\overline{\rho}_i = 1$  corresponds to the closed conformation and  $\Delta\overline{\rho}_i = -1$  corresponds to the open conformation of nCaM or cCaM. The transition routes illustrated by  $\Delta\overline{\rho}_i$  for each residue of nCaM and cCaM are shown in Fig. 2(b) and Fig. 3(b), respectively. Fig. 3(b) illustrates the conformational transition of cCaM in terms of  $\Delta\overline{\rho}_i$  for each residue. As shown in Fig. 3(b), the model predicts that the structural change in binding loop II occurs earlier than binding loop III during the domain opening of cCaM. [See the sharp change in color near residue number 130 in Fig. 3(b)]. Also, helix G has an earlier conformational transition than helix F (Fig. 3(b)). This sequence is quite different from nCaM as shown in Fig. 2(b). For nCaM the structural change in helix B is predicted to be earlier than the structural change in helix C for the closed to open conformational transition. Finally, when we compared the structural change in the helix-linker of the two domains, our results show F/G helix-linker in the cCaM has abrupt transition near the open state. [See the transition near residue number 115 in Fig. 3(b).] This may have some implication for cracking in the F/G helix-linker region of cCaM. In contrast, the transition in the B/C helix-linker in nCaM is more gradual (see Fig. 2(b)).

**Conformational Flexibility and Cracking of the CaM2/3 Fragment.** The engineered “even-odd” EF-hands paired CaM2/3 fragment (composed of EF-hands 2 and 3) has been shown recently to have distinct transition characteristics from the “odd-even” EF-hands paired nCaM and cCaM.<sup>15</sup> NMR spectroscopy has shown that  $\text{Ca}^{2+}$ -free (apo) CaM2/3 does not have a stable folded structure but rather shows characteristics of a molten globule state.  $\text{Ca}^{2+}$  binding induces the folding of this “even-odd” paired EF-hand motifs CaM2/3 and the  $\text{Ca}^{2+}$ -bound (holo) CaM2/3 adopts a similar structure as holo-nCaM or cCaM (see PDB ID *2hf5*).<sup>15</sup> In contrast to the  $\text{Ca}^{2+}$ -CaM (holo-CaM) structure, the  $\text{Ca}^{2+}$ -CaM2/3 structure does not have a stable helix in the central linker region. In our model, we study the two meta-stable conformations, apo-CaM2/3 and holo-CaM2/3 were taken directly from the folded apo-CaM (PDB ID *1cfd*) and holo-CaM (PDB ID *1cfl*) respectively. Here, we focus mainly on the conformational flexibility and transition of the central linker to a stable  $\alpha$ -helix. This central linker of CaM was also previously studied by MD simulation.<sup>18</sup> Even though our model does not accommodate all the relevant conditions of the NMR experiment reported in Ref. 15, the model does capture certain aspects of the the apo/holo

conformational transition of this CaM2/3 fragment. In particular, the model predicts a apo-CaM2/3 to the holo-CaM2/3 conformational transition mechanism that agrees well with the sequential  $\text{Ca}^{2+}$  binding mechanism of CaM2/3 suggested by the NMR measurements.

The magnitude of the fluctuations of each residue in CaM2/3 [shown in Fig. 6(a)] suggests that the change in conformational flexibility of binding loops II and III of CaM2/3 are very different. In particular, helix C and binding loop II are highly flexible in the apo conformation of CaM2/3. This very high intrinsic flexibility of apo-CaM2/3 may account for the molten globule state characteristics described in Ref. 15. Fig. 6(a) also shows that binding loop II is more flexible than loop III. This result is in harmony with the NMR measurements of  $\text{Ca}^{2+}$  binding in CaM2/3<sup>15</sup> that shows  $\text{Ca}^{2+}$  binds to loop III with higher affinity (lower  $\text{Ca}^{2+}$  concentration) than loop II. Our results also indicate that the flexibility of binding loop III decreases monotonically along the transition route from the apo-CaM2/3 to the holo-CaM2/3 structure. In contrast, the flexibility of helix F increases along the transition route from apo to holo transition of CaM2/3 fragment. In particular, N-terminal part (close to binding loop III) of helix F partially unfolds when adopting the holo-CaM2/3 conformation. We also notice in Fig. 6(a) that the domain linker between EF-hands 2 and 3 (residue number 74-81) during the apo to holo transition has a relatively large change in conformational flexibility. The fluctuation amplitude  $\mathcal{B}_i$  of this linker increases in the intermediate states and then decrease abruptly as the helix forms near the holo state. The local unfolding of the domain linker enhances the flexibility of this linker region dramatically, first relaxing in structure and then stabilized in the holo-CaM2/3 structure as a rigid  $\alpha$ -helix conformation. This local unfolding signaled by increase and decrease in flexibility is similar to the cracking exhibited in cCaM.

Local intermediate unfolding (i.e., cracking ) of the domain linker during the apo to holo transition of CaM2/3 can also be seen through change in the pair potential energy  $u_{ij}$  for the Aspartic (Asp) residue from the linker at position 80 along the transition route as shown in Fig. 7. During the apo to holo transition of CaM2/3 the energy of residue Asp80 increases from the apo-CaM2/3 structure ( $\alpha = 1$ ) and decreases abruptly at the transition state ( $\alpha_0 = 0.4$ ) to the minimum at holo-CaM2/3 structure ( $\alpha_0 = 0$ ) as the helix forms . This increase and then sharp decrease in the contact energy of residue Asp80 signals cracking (local unfolding and refolding) of the linker in CaM2/3 to a stable  $\alpha$ -helix. We note also that the energy relative to the holo-CaM2/3 energy of Asp80 is higher than that of

Asp118 from the F/G helix-linker of cCaM. This emphasizes the importance of cracking in the apo-CaM2/3 to holo-CaM2/3 transition.

**Conformational Transition Mechanism of CaM2/3 Fragment.** For CaM2/3, the order parameter  $\Delta\overline{\rho}_i = 1$  corresponds to the apo state and  $\Delta\overline{\rho}_i = -1$  corresponds to the holo state of CaM2/3. The abrupt and early change in  $\Delta\overline{\rho}_i = 1$  for residues in the domain linker (sequence number 74-81) illustrated in Fig. 6(b) clearly shows the transition of the flexible inter domain linker to a rigid  $\alpha$ -helix as discussed above in terms of the fluctuations  $\{\mathcal{B}_i\}$ . Fig. 6(b) also indicates that the structural change in binding loop III is initiated earlier than the structural change in binding loop II. Also, the conformational change in binding loop II is much more gradual than that of binding loop III. Similar to the identification of the  $\text{Ca}^{2+}$  binding affinity with the changes in inherent flexibility, the early structural change in binding loop III may imply the stepwise binding of  $\text{Ca}^{2+}$  in CaM2/3 with loop III having a higher binding affinity than loop II.

## DISCUSSION

CaM, a small (148-residue)  $\text{Ca}^{2+}$ -binding protein with very high plasticity, may be an ideal system to demonstrate flexibility influenced conformational transitions. The protein consists of structurally similar N- and C-terminal globular domains connected by a flexible tether also known as central or interdomain linker.<sup>19</sup> The  $\text{Ca}^{2+}$  induced structural rearrangement in CaM result in the solvent exposure of large hydrophobic surface responsible for molecular recognition of various cellular targets.<sup>20</sup>

While similar in structure and fold, the two CaM domains are quite different in terms of their flexibility, melting temperatures, and  $\text{Ca}^{2+}$ -binding affinities.<sup>6,7</sup> In the two homologous (46% sequence identity) domains of CaM,  $\text{Ca}^{2+}$  binding occurs sequentially. First, in the binding sites of cCaM and then in the binding sites of nCaM.<sup>6</sup> In spite of large cooperativity in the  $\text{Ca}^{2+}$  binding process within each domain the two domains reflect different  $\text{Ca}^{2+}$  and target affinities. The N-terminal pair of EF-hands binds to  $\text{Ca}^{2+}$  ions with much lower affinity than the C-terminal EF-hands pair.<sup>6</sup> Nuclear Magnetic Resonance (NMR)<sup>21,22</sup> and molecular-dynamics (MD) simulation<sup>23</sup> studies have shown that the  $\text{Ca}^{2+}$ -bound nCaM is considerably less open than the cCaM. This was not observed in the X-ray crystal structure of the protein. Experimentally it has been shown that the more-conserved cCaM has a



greater affinity for  $\text{Ca}^{2+}$  and some CaM targets, whereas the nCaM is less specific in its choice of target motif.<sup>24,25</sup> Heat denaturation studies have shown that cCaM of  $\text{Ca}^{2+}$ -free (apo) CaM starts to denature slightly above the physiological temperature.<sup>7</sup> The denaturation of the apo-cCaM was observed at lower concentration of denaturant than denaturation of the nCaM, while the order was reversed for  $\text{Ca}^{2+}$ -CaM.<sup>26</sup> From temperature-jump fluorescence spectroscopy by Rabl et al.<sup>27</sup> the instability of the cCaM was also observed from the study of unfolding of apo-CaM. They suggested that the cCaM was partially unfolded at native conditions. Recent NMR experiments done by Lundstrom and Akke<sup>28</sup> monitoring relaxation rates involving  $^{13}\text{C}^\alpha$  spins in adjacent residues of E140Q mutant of cCaM revealed transient partial unfolding of helix F. This was interpreted as a global exchange process involves a partially unfolded minor state that was not detected previously<sup>22,29</sup>. A very recent conformational dynamics simulation of the cCaM by Chen et al.<sup>30</sup> has shown presence of an unfolded apo-state. These observations further suggests that the conformational exchange may be more complex than a simple two-state process.

The variational model presented in this paper agrees with the emphasis on differences in inherent flexibility of the two domains to understand their distinct physical characteristics and the complexity in the conformational transition mechanism.<sup>21</sup> Our results also agree with a MD simulation study<sup>31</sup> which has shown that the nCaM is inherently more flexible with lower binding affinity than the cCaM. The more open conformation and lower intrinsic flexibility of the cCaM is also probably the key to understanding initial binding between this domain and CaM’s target enzymes.<sup>31,32</sup>

The variational model presented in this paper predicts that the different inherent flexibilities of the two domains of CaM also lead to distinct transition mechanisms, even though the folded state topology of the two domains is the same. The mechanism controlling the open/closed transition does not involve cracking for the relatively flexible nCaM whereas the mechanism controlling the conformation transition of the more rigid cCaM exhibits transient partial local unfolding in its helix-linker between the binding loops. This partial local unfolding or cracking in the cCaM shows the complexity of the open/closed conformational transition mechanism of cCaM.

A recent NMR experiment studied the EF-hand association affects on the structure,  $\text{Ca}^{2+}$  affinity, and cooperativity of CaM.<sup>15</sup> The EF-hands in CaM domains are “odd-even” paired with EF-hands 1 and 2 in nCaM and EF-hands 3 and 4 in cCaM. This arrangement

of EF-hands in CaM is thought to be a consequence of its evolution from a biologically related ancestor EF-hand by gene duplication.<sup>33</sup> The “even-odd” pairing of EF-hands 2 and 3 (CaM2/3) (Fig. 1(c)) has been characterized by NMR in Ref. 15. In this fragment, EF-hands 2 and 3 are connected by the central linker between nCaM and cCaM. Although, from the crystal structure of holo  $\text{Ca}^{2+}$ -CaM this interdomain linker region is observed to be a long rigid  $\alpha$ -helix,<sup>34</sup> several NMR relaxation experiments have demonstrated that this central linker is flexible in solution near its midpoint and the two domains do not interact.<sup>18,19</sup> In contrast to the high affinity and positive cooperativity for  $\text{Ca}^{2+}$  binding in the two “odd-even” paired EF-hand domains of CaM, the CaM2/3 binds  $\text{Ca}^{2+}$  in a sequence. First in the high-affinity EF-hand 3 and then in the EF-hand 2 with much lower affinity.<sup>15</sup> Although not a direct focus of our paper, we also note that a peptide binding to CaM2/3 has also been characterized recently by McIntosh and co-workers.<sup>35</sup> It was found that CaM2/3 adopts  $\text{Ca}^{2+}$ -bound structure with peptide binding very much similar to those of nCaM or cCaM. These observations reflect the very high plasticity of the EF-hand association and mediate  $\text{Ca}^{2+}$ -dependent recognition of target proteins.

Our results of apo/holo conformational transition of CaM2/3 reveals that the central linker in CaM2/3 is highly flexible and dominates the transition mechanism. The folding of this linker to a rigid  $\alpha$ -helix is preceded by a further increase in its flexibility and local unfolding. This cracking leads to a very sharp transition of the helix-linker from apo-CaM2/3 to holo-CaM2/3 conformation. While our model did not predict partial local unfolding or cracking of helix-F from the open/closed conformational transition of cCaM, the apo/holo conformational transition of CaM2/3 reveals cracking in some region of helix-F as we have discussed already in comparison with the NMR study<sup>28</sup>. The predicted change in conformational flexibility of CaM2/3 reveals the stepwise binding of  $\text{Ca}^{2+}$  ions with binding loop III having higher affinity than binding loop II. Furthermore, our results suggests that due to very high inherent flexibility the central linker in CaM2/3 behaves more like a helix-linker in CaM domains, as concluded from NMR measurements.<sup>15</sup> On the other hand, in  $\text{Ca}^{2+}$ -bound (holo) CaM structure<sup>36</sup> this same central linker adopts a more stable  $\alpha$ -helix conformation which requires cracking in the conformational transition from its apo-CaM structure.

## METHODS

**Preparation of Structures.** The structures of the two conformations of the transition are rotated to have the same center of mass and minimum root-mean square deviation of the  $C_\alpha$  positions. In nCaM, EF-hands 1 and 2 are consist of helices A/B and C/D (Fig. 1(a)), respectively, whereas helices E/F and G/H in cCaM (Fig. 1(b)) form EF-hands 3 and 4, respectively. The fragment CaM2/3 contains EF-hands 2 and 3 with helices C/D and E/F (Fig. 1(c)), respectively. The conformational transition in cCaM is modeled from the residues 76-147 of apo-CaM (PDB ID *1cfd*)<sup>37</sup> and holo-CaM (PDB ID *1cll*)<sup>36</sup> structures, while the conformational transition in nCaM is modeled from the residues 4-75 of the same PDB structures. The apo to holo conformational transition of the “even-odd” paired EF-hand motifs CaM2/3 are modeled from EF-hands 2 and 3, residues 46-113 of apo-CaM (PDB ID *1cfd*) and holo-CaM (PDB ID *1cll*) structures.

**The Variational Model of Conformational Transitions.** A conformation of a protein in our model (described in more detail in Ref.16) is described by the  $N$  position vectors of the  $\alpha$ -carbons of the polypeptide backbone,  $\{\mathbf{r}_i\}$ . Partially ordered ensembles of polymer configurations are described by a coarse-grained reference Hamiltonian

$$\mathcal{H}_0/k_B T = \mathcal{H}_{\text{chain}}/k_B T + \frac{3}{2a^2} \sum_i C_i [\mathbf{r}_i - \mathbf{r}_i^N(\alpha_i)]^2, \quad (1)$$

where  $T$  is the temperature and  $k_B$  is Boltzmann’s constant. Here,  $\mathcal{H}_{\text{chain}}$  is a harmonic potential that enforces chain connectivity of a freely rotating polymer with mean bond length  $a = 3.8\text{\AA}$ ,<sup>38</sup> and mean valance angle  $\cos\theta = 0.8$ .<sup>39</sup> The second term includes  $N$  variational parameters,  $\{C_i\}$ , that control the magnitude of the fluctuations about  $\alpha$ -carbon position vectors

$$\mathbf{r}_i^N(\alpha_i) = \alpha_i \mathbf{r}_i^{N_{\text{apo}}} + (1 - \alpha_i) \mathbf{r}_i^{N_{\text{holo}}}. \quad (2)$$

Here, we have introduced another set of  $N$  variational parameters,  $\{\alpha_i\}$  ( ranging between 0 and 1), that specify the backbone positions as an interpolation between the apo-CaM and holo-CaM conformations,  $\{\mathbf{r}_i^{N_{\text{apo}}}\}$  and  $\{\mathbf{r}_i^{N_{\text{holo}}}\}$ , respectively. The probability for a particular configurational ensemble specified by the variational parameters  $\{C_i, \alpha_i\}$  at temperature  $T$  is given by the variational free energy  $F(\{C\}, \{\alpha\}) = E(\{C\}, \{\alpha\}) - TS(\{C\}, \{\alpha\})$ . Here,  $S(\{C\}, \{\alpha\})$  is the entropy loss due to the localization of the residues around the mean positions  $\{\mathbf{r}_i(\alpha_i)\}$ . The energy is determined by the two-body interactions between distant

residues  $E(\{C\}, \{\alpha\}) = \sum_{[i,j]} \epsilon_{ij} u_{ij}$ , where  $u_{ij}$  is the average of the pair potential  $u(r_{ij})$  over  $\mathcal{H}_0$ ,<sup>38</sup> and  $\epsilon_{ij}$  is the strength of a fully formed contact between residues  $i$  and  $j$  given by Miyazawa-Jernigan interaction parameters.<sup>40</sup> The sum is restricted to a set of contacts  $[i, j]$  determined by pairs of residues in the proximity in each of the meta-stable conformations.<sup>16</sup> Each meta-stable conformation has a distinct but overlapping set of contacts  $[i, j]_{\text{apo}}$ ,  $[i, j]_{\text{holo}}$  and  $[i, j]$  is the union of these sets of contacts. In this model, the interaction energy for contacts that occur exclusively in only one meta-stable structure is given by  $\exp(-u_{ij}/k_B T) = 1 + \exp(-\langle u_{ij} \rangle_0 / k_B T)$ . This two-state model provides an interpolation at the individual contact level of the interaction energy determined by the two meta-stable conformations and is similar to some other native state biased potentials describing conformational transitions.<sup>10,11,12</sup>

Analysis of the free energy surface parameterized by  $\{C, \alpha\}$  follows the program developed to describe folding:<sup>38</sup> the mechanism controlling the kinetics of the transitions is determined by the ensemble of structures characterized by the monomer density at the saddlepoints of the free energy. At this point, we simplify our model and restrict the interpolation parameter  $\alpha_i$  to be the same for all residues,  $\alpha_i = \alpha_0$ .<sup>41</sup> With this simplification, the numerical problem of finding saddle-points with respect to  $\{C, \alpha\}$  simplifies to minimizing the free energy  $F(\{C\}, \alpha_0)$  with respect to  $\{C\}$  for a fixed  $\alpha_0$ .

**Conformational Flexibility.** Main-chain conformational flexibility is characterized by the mean-square fluctuations  $\{\mathcal{B}_i(\alpha_0)\}$  of each  $\alpha$ -carbon of the polypeptide chain from its average positions,  $\delta \mathbf{r}_i$ , along the transition route as  $\alpha$  goes from 0 to 1.<sup>16</sup> These natural order parameters for the reference Hamiltonian  $\mathcal{H}_0$ ,  $\mathcal{B}_i = \langle \delta \mathbf{r}_i^2 \rangle_0$ , contains information about the degree of structural order of each residue.<sup>8,38</sup>

**Conformational Transition Mechanism.** The main-chain dynamics responsible for the detailed mechanism of the conformational transition in our analysis is based on the order parameters introduced to describe the folding mechanism  $\rho_i^{\text{apo/holo}} = \langle \exp(-\alpha^N (\mathbf{r}_i - \mathbf{r}_i^{\text{N}_{apo/holo}})^2)_0$  with  $\alpha^N = 0.5$  defining the width of a Gaussian window about the meta-stable structure  $\{\mathbf{r}_i^{\text{N}_{apo/holo}}\}$ . In particular, it is convenient to characterize the relative similarity to the apo structure along the transition route through the normalized measure

$$\overline{\rho}_i^{\text{apo}}(\alpha_0) = \frac{\rho_i^{\text{apo}}(\alpha_0) - \rho_i^{\text{apo}}(0)}{\rho_i^{\text{apo}}(1) - \rho_i^{\text{apo}}(0)}, \quad (3)$$

where  $\rho_i^{\text{apo}}(\alpha_0)$  is the monomer density of the  $i^{\text{th}}$  residue with respect to the apo conformation

described by  $\{\mathbf{r}_i^{N_{\text{apo}}}\}^{16}$ . Similarly, we represent the relative structural similarity to the holo conformation as

$$\overline{\rho}_i^{\text{holo}}(\alpha_0) = \frac{\rho_i^{\text{holo}}(\alpha_0) - \rho_i^{\text{holo}}(1)}{\rho_i^{\text{holo}}(0) - \rho_i^{\text{holo}}(1)}, \quad (4)$$

where  $\rho_i^{\text{holo}}(\alpha_0)$  is the monomer density of the  $i^{\text{th}}$  residue with respect to the holo conformation described by  $\{\mathbf{r}_i^{N_{\text{holo}}}\}$ . In the holo state,  $\overline{\rho}_i^{\text{apo}}(0) = 0$  and  $\overline{\rho}_i^{\text{holo}}(0) = 1$ , while in the apo state  $\overline{\rho}_i^{\text{apo}}(1) = 1$  and  $\overline{\rho}_i^{\text{holo}}(1) = 0$ . To represent the structural changes more clearly, it is convenient to consider the difference,

$$\Delta\overline{\rho}_i(\alpha_0) = \overline{\rho}_i^{\text{apo}}(\alpha_0) - \overline{\rho}_i^{\text{holo}}(\alpha_0) \quad (5)$$

for each residue. This difference shifts the relative degree of localization to be between  $\Delta\overline{\rho}_i(1) = 1$  and  $\Delta\overline{\rho}_i(0) = -1$  corresponding to the apo and holo conformations, respectively.

## REFERENCES

---

- <sup>1</sup> G. Weber, *Biochemistry* **11**, 864 (1972).
- <sup>2</sup> O. Miyashita, J. N. Onuchic, and P. G. Wolynes, *Proc. Natl. Acad. Sci. USA* **100**, 12570 (2003).
- <sup>3</sup> O. Miyashita, P. G. Wolynes, and J. N. Onuchic, *J. Phys. Chem. B* **109**, 1959 (2005).
- <sup>4</sup> J. D. Bryngelson, J. N. Onuchic, N. D. Socci, and P. G. Wolynes, *Proteins Struct. Funct. Genet.* **21**, 167 (1995).
- <sup>5</sup> J. N. Onuchic and P. G. Wolynes, *Curr. Opin. Struct. Biol.* **14**, 70 (2004).
- <sup>6</sup> S. Linse, A. Helmersson, and S. Forsen, *J. Biol. Chem.* **266**, 8050 (1991).
- <sup>7</sup> T. N. Tsalkova and P. L. Privalov, *J. Mol. Biol.* **181**, 533 (1985).
- <sup>8</sup> J. J. Portman, S. Takada, and P. G. Wolynes, *Phys. Rev. Lett.* **81**, 5237 (1998).
- <sup>9</sup> D. M. Zuckerman, *J. Phys. Chem. B* **108**, 5127 (2004).
- <sup>10</sup> R. B. Best, Y. G. Chen, and G. Hummer, *Structure* **13**, 1755 (2005).
- <sup>11</sup> P. Maragakis and M. Karplus, *J. Mol. Biol.* **352**, 807 (2005).
- <sup>12</sup> K. Okazaki, N. Koga, S. Takada, J. N. Onuchic, and P. G. Wolynes, *Proc. Natl. Acad. Sci. USA* **103**, 11844 (2006).
- <sup>13</sup> P. C. Whitford, O. Miyashita, Y. Levy, and J. N. Onuchic, *J. Mol. Biol.* **366**, 1661 (2007).
- <sup>14</sup> J.-W. Chu and G. A. Voth, *Biophys. J.* **93**, 3860 (2007).
- <sup>15</sup> T. M. Lakowski, G. M. Lee, M. Okon, R. E. Reid, and L. P. McIntosh, *Protein Sci.* **16**, 1119 (2007).
- <sup>16</sup> S. Tripathi and J. J. Portman, *J. Chem. Phys.* **128**, 205104 (2008).
- <sup>17</sup> V. A. Likic, E. E. Strehler, and P. R. Gooley, *Protein Sci.* **12**, 2215 (2003).
- <sup>18</sup> D. van der Spoel, B. L. de Groot, S. Hayward, H. J. Berendsen, and H. J. Vogel, *Protein Sci.* **5**, 2044 (1996).
- <sup>19</sup> G. Barbato, M. Ikura, L. E. Kay, R. W. Pastor, and A. Bax, *Biochemistry* **31**, 5269 (1992).
- <sup>20</sup> W. E. Meador, A. R. Means, and F. A. Quiocho, *Science* **262**, 1718 (1993).
- <sup>21</sup> J. J. Chou, S. Li, C. B. Klee, and A. Bax, *Nat. Struct. Biol.* **8**, 990 (2001).
- <sup>22</sup> J. Evenas, S. Forsen, A. Malmendal, and M. Akke, *J. Mol. Biol.* **289**, 603 (1999).
- <sup>23</sup> D. Vigil, S. C. Gallagher, J. Trehwella, and A. E. Garcia, *Biophys. J.* **80**, 2082 (2001).
- <sup>24</sup> P. M. Baley, W. A. Findlay, and S. R. Martin, *Protein Sci.* **5**, 1215 (1996).

- <sup>25</sup> A. Barth, S. R. Martin, and P. M. Bayley, *J. Biol. Chem.* **273**, 2174 (1998).
- <sup>26</sup> L. Masino, S. R. Martin, and P. M. Bayley, *Protein Sci.* **9**, 1519 (2000).
- <sup>27</sup> C.-R. Rabl, S. R. Martin, E. Neumann, and P. M. Bayley, *Biophys. Chem.* **101**, 553 (2002).
- <sup>28</sup> P. Lundstrom, F. A. A. Mulder, and M. Akke, *Proc. Natl. Acad. Sci. USA* **102**, 16984 (2005).
- <sup>29</sup> J. Evenas, A. Malmendal, and M. Akke, *Structure* **9**, 185 (2001).
- <sup>30</sup> Y.-G. Chen and G. Hummer, *J. Am. Chem. Soc.* **129**, 2414 (2007).
- <sup>31</sup> N. P. Barton, C. S. Verma, and L. S. D. Caves, *J. Phys. Chem. B* **106**, 11036 (2002).
- <sup>32</sup> A. P. Yamniuk and H. J. Vogel, *Molecular Biotechnology* **27**, 33 (2004).
- <sup>33</sup> S. Nakayama, N. D. Moncrief, and R. H. Kretsinger, *J. Mol. Evol.* **34**, 416 (1992).
- <sup>34</sup> Y. S. Babu, S. Sack, T. J. Greenhough, C. E. Bugg, A. R. Means, and W. J. Cook, *Nature* **315**, 37 (1985).
- <sup>35</sup> T. M. Lakowski, G. M. Lee, B. Lelj-Garolla, M. Okon, R. E. Reid, and L. P. McIntosh, *Biochemistry* **46**, 8525 (2007).
- <sup>36</sup> R. Chattopadhyaya, W. E. Meador, A. R. Means, and F. A. Quiocho, *J. Mol. Biol.* **228**, 1177 (1992).
- <sup>37</sup> H. Kuboniwa, N. Tjandra, S. Grzesiek, H. Ren, C. B. Klee, and A. Bax, *Nat. Struct. Biol.* **2**, 768 (1995).
- <sup>38</sup> J. J. Portman, S. Takada, and P. G. Wolynes, *J. Chem. Phys.* **114**, 5069 (2001).
- <sup>39</sup> M. Bixon and R. Zwanzig, *J. Chem. Phys.* **68**, 1896 (1978).
- <sup>40</sup> S. Miyazawa and R. L. Jernigan, *J. Mol. Biol.* **256**, 623 (1996).
- <sup>41</sup> M. K. Kim, R. L. Jernigan, and G. S. Chirikjian, *Biophys. J.* **83**, 1620 (2002).
- <sup>42</sup> W. Humphrey, A. Dalke, and K. Schulten, *J. Mol. Graphics* **14**, 33 (1996).

## Figure Legends

*Figure 1.*

Three dimensional structures of calmodulin (CaM) domains and EF-hands 2 and 3 fragment. The apo-CaM and holo-CaM structures shown here correspond to human CaM with PDB code *1cfd* and *1cfl* respectively. (a) The closed, apo and open, holo conformations of N-terminal domains of CaM (nCaM) consist of helices A/B and C/D with binding loops I and II respectively. (b) The closed, apo and open, holo conformations of C-terminal domains of CaM (cCaM) consist of helices E/F and G/H with binding loops III and IV respectively. (c) The unfolded (apo) and folded (holo) EF-hands of CaM (CaM2/3) consist of helices C/D and E/F with binding loops II and III respectively. These three-dimensional illustrations were made using Visual Molecular Dynamics (VMD).<sup>42</sup>

*Figure 2.*

(a) Fluctuations  $\mathcal{B}_i$  vs residue index of N-domain of CaM (nCaM) for selected values of the interpolation parameter  $\alpha_0$  in the conformational transition route between open and closed structures. The secondary structure of nCaM is indicated above the plot. Helices are represented by the rectangular boxes, binding loops and helix-linker are by lines and small  $\beta$ -sheets are by arrows. (b) Difference between the normalized native density  $\Delta\overline{\rho}_i$  (a measure of structural similarity) of each residue for different  $\alpha_0$ . The change in color from red to blue is showing the closed to open conformational transition of nCaM. This is normalized to be  $-1$  at the open state minimum ( $\alpha_0 = 0$ ; blue) and  $1$  at the closed state minimum ( $\alpha_0 = 1$ ; red).

*Figure 3.*

(a) Fluctuations  $\mathcal{B}_i$  vs residue index of C-domain of CaM (cCaM) for selected values of the interpolation parameter  $\alpha_0$  in the conformational transition route between open and closed structures. The secondary structure of cCaM is indicated above the plot. (b) Difference between the normalized native density  $\Delta\overline{\rho}_i$  (a measure of structural similarity) of each residue for different  $\alpha_0$ . The change in color from red to blue is showing the closed to open



conformational transition of cCaM. This is normalized to be  $-1$  at the open state minimum ( $\alpha_0 = 0$ ; blue) and  $1$  at the closed state minimum ( $\alpha_0 = 1$ ; red).

*Figure 4.*

Change in fluctuations  $\mathcal{B}_i$  of the residues from binding loops and helix-linker of CaM domains along the open/closed conformational transition route for different  $\alpha_0$ . Residues Gly23, Gly59 and Glu45 are from binding loop I, loop II and the helix-linker of the nCaM, respectively. While, residues Gly96, Gly132 and Asp118 are from binding loop III, loop IV and the helix-linker of the cCaM, respectively.

*Figure 5.*

Average pair potentials  $u_{ij}$  of the residues from the helix-linker of CaM domains along the open/closed conformational transition route for different  $\alpha_0$ . Residue Glu45 and Asp118 are from the nCaM and cCaM, respectively.

*Figure 6.*

(a) Fluctuations  $\mathcal{B}_i$  vs residue index of fragment EF-hands 2 and 3 of CaM (CaM2/3) for selected values of the interpolation parameter  $\alpha_0$  in the conformational transition route between unfolded and folded states. The secondary structure of CaM2/3 is indicated above the plot. (b) Difference between the normalized native density  $\Delta\bar{\rho}_i$  (a measure of structural similarity) of each residue for different  $\alpha_0$ . The change in color from red to blue is showing the unfolded to folded conformational transition of CaM2/3. This is normalized to be  $-1$  at the folded state minimum ( $\alpha_0 = 0$ ; blue) and  $1$  at the unfolded state minimum ( $\alpha_0 = 1$ ; red).

*Figure 7.*

Average pair potentials  $u_{ij}$  of the residues Asp80 from the central linker of CaM along the open/closed conformational transition route for different  $\alpha_0$ .

# Figures

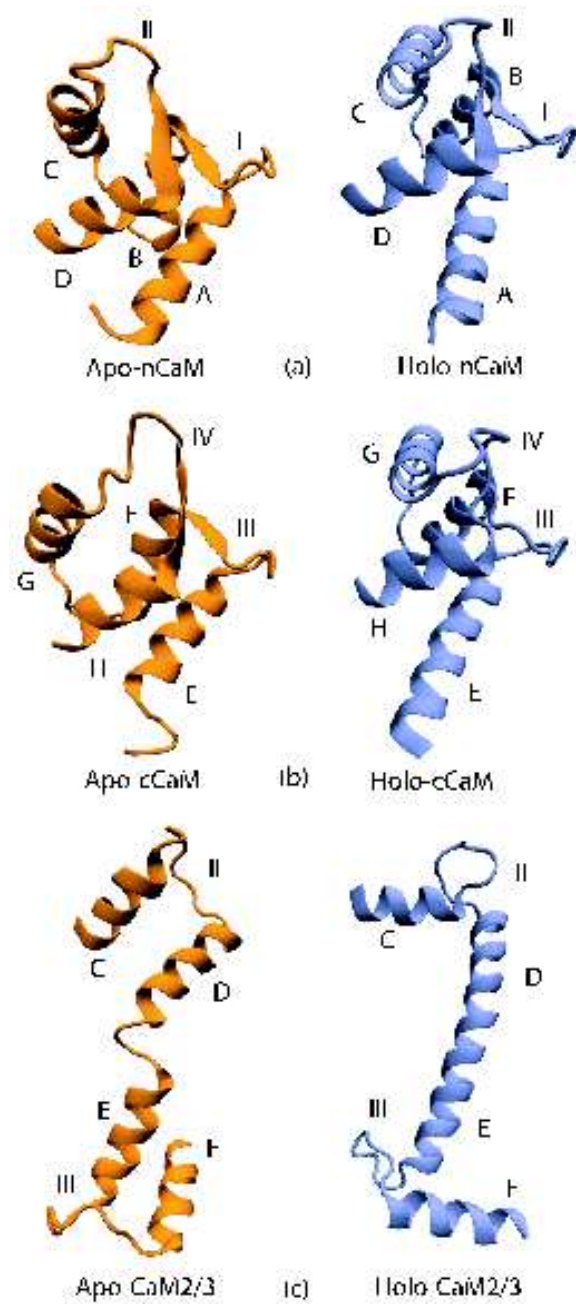


FIG. 1:

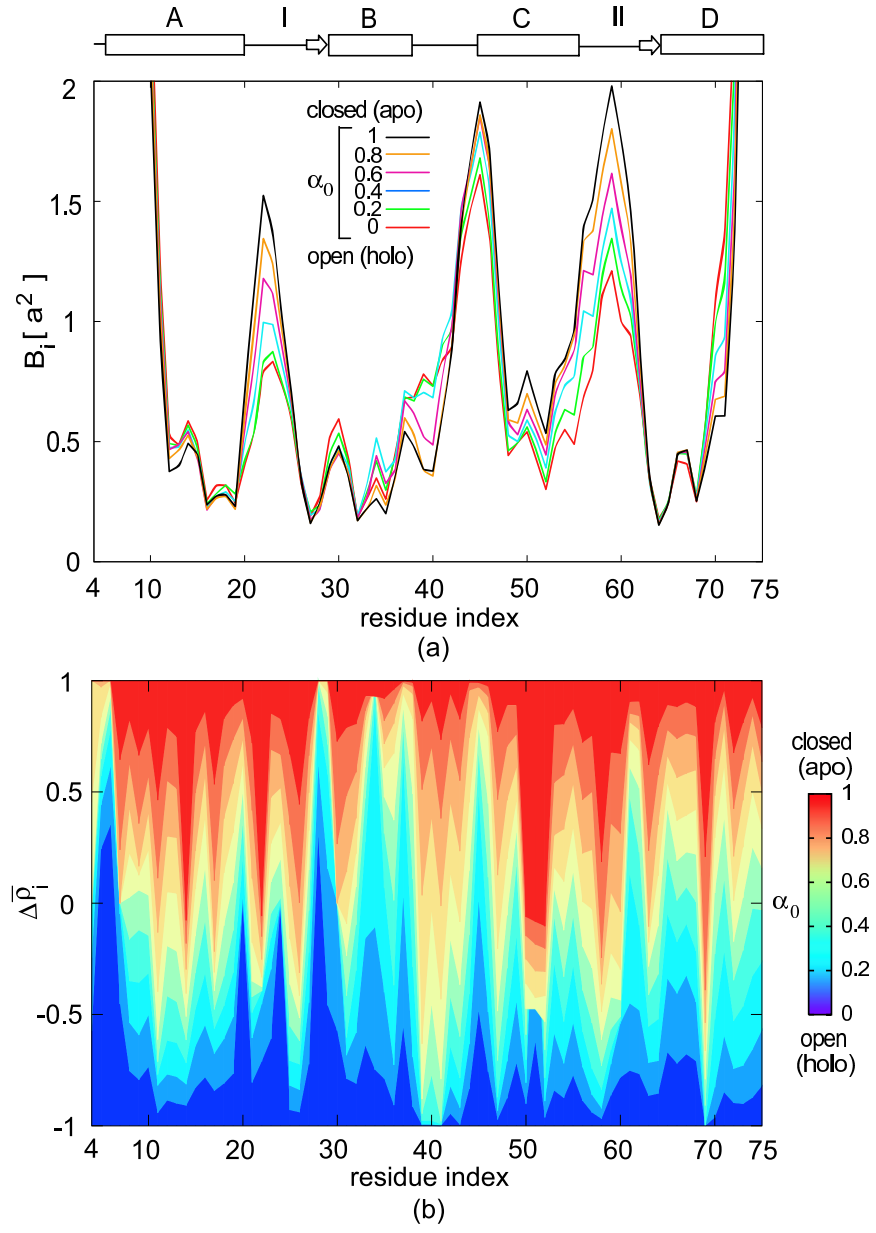


FIG. 2:

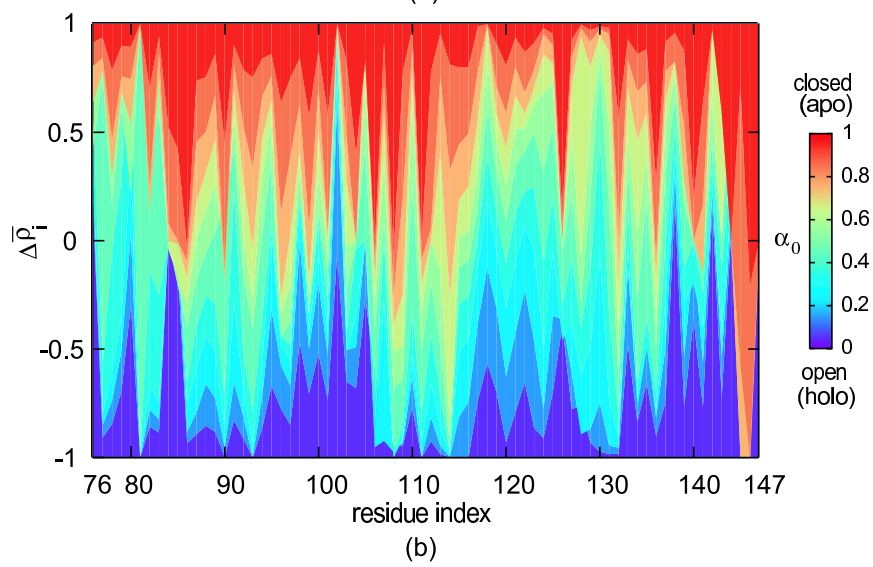
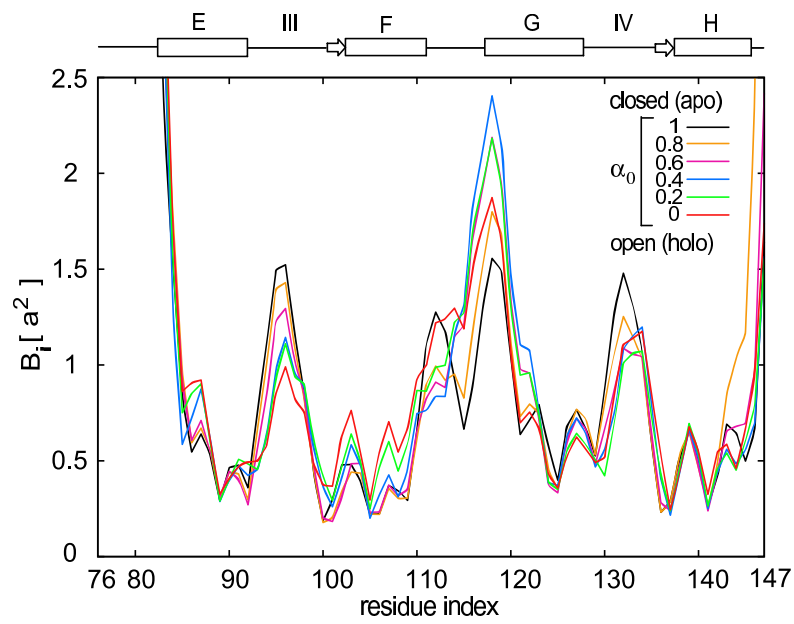


FIG. 3:

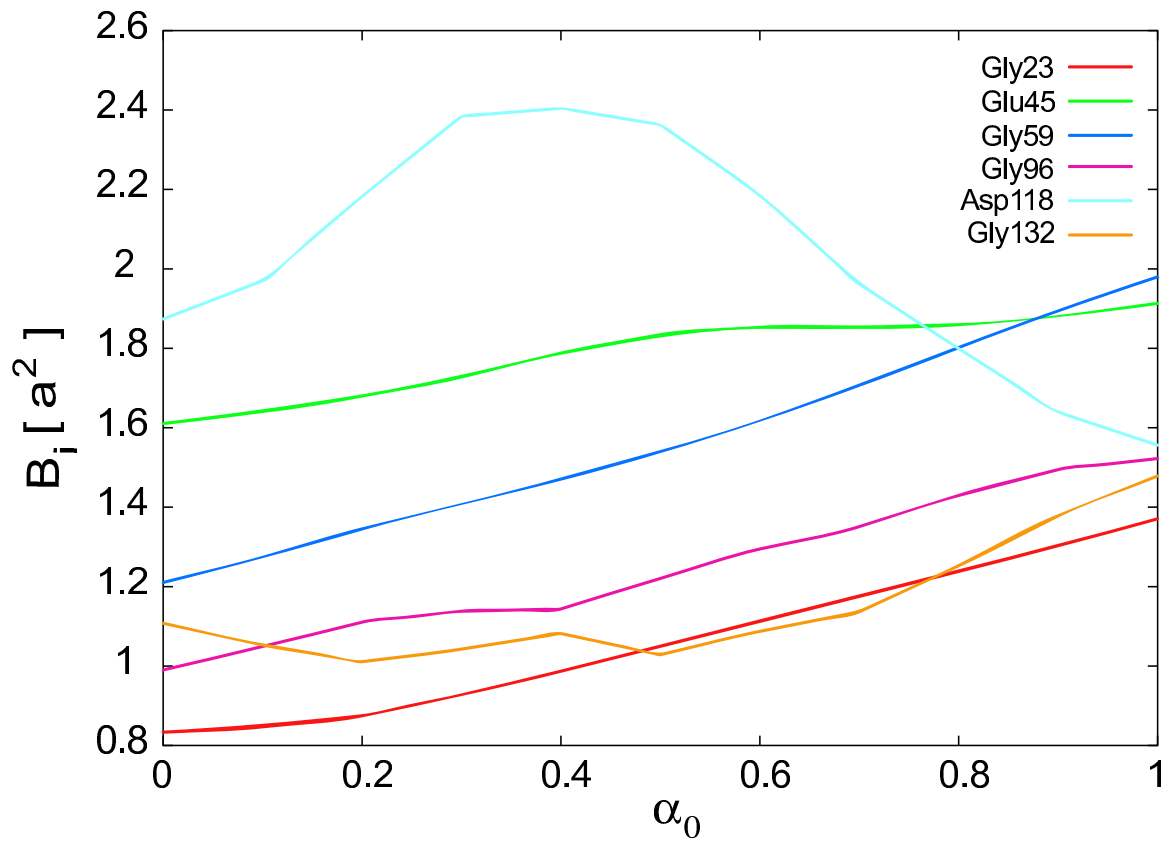


FIG. 4:

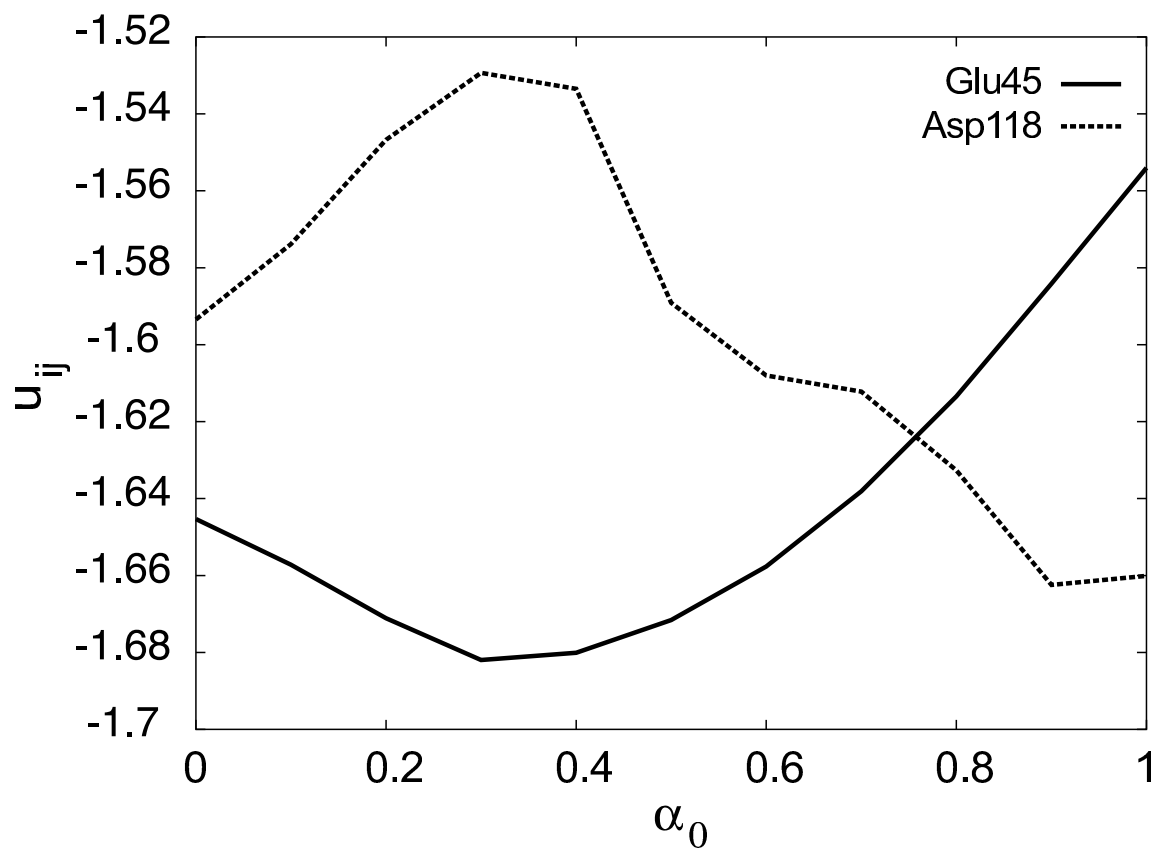


FIG. 5:

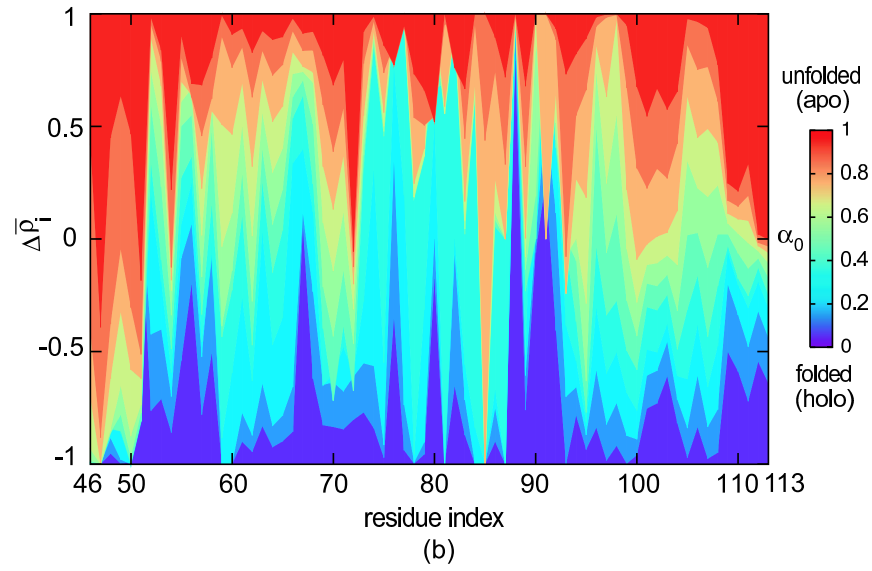
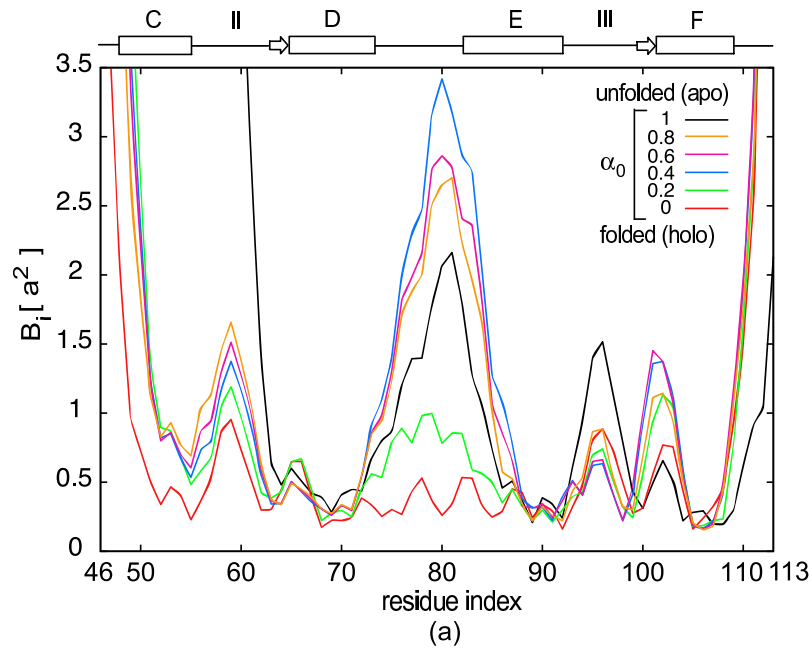


FIG. 6:

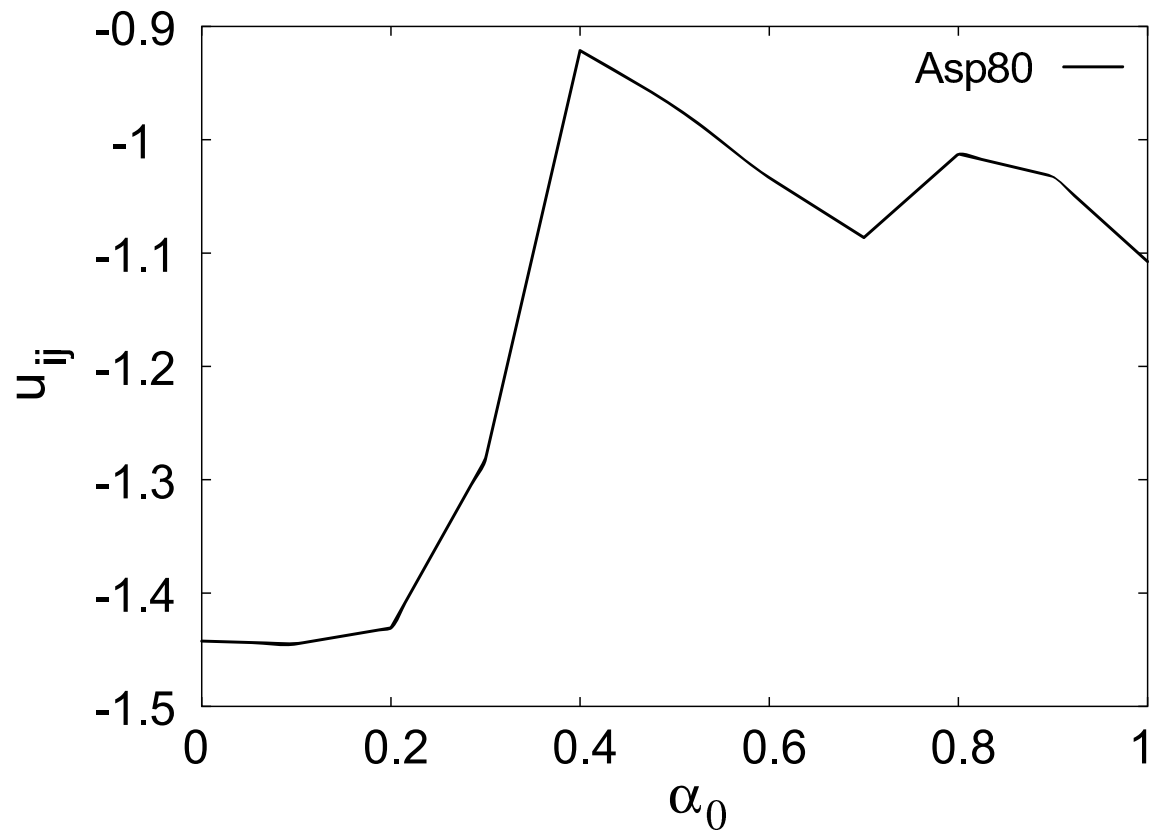


FIG. 7: